JOURNAL OF SOLID STATE CHEMISTRY **122,** 259–265 (1996)
ARTICLE NO. 0111

Modeling of Extended Defects in the Vanadium Phosphate Catalyst for Butane Oxidation, $(VO)_2P_2O_7$

P. T. Nguyen and A. W. Sleight[1]

Department of Chemistry, Oregon State University, Corvallis, Oregon 97331-4003

and

N. Roberts and W. W. Warren

Department of Physics, Oregon State University, Corvallis, Oregon 97331-6502

Received September 6, 1995; in revised form December 15, 1995; accepted December 19, 1995

X-ray diffraction patterns of catalysts based on $(VO)_2P_2O_7$ show peak broadening effects which cannot be explained by strain and crystallite size effects. We show that the extensive broadening of peaks where the *h* or *l* indices are odd is due to extended defects. These defects can be modeled as stacking faults perpendicular to the a and c axes. The proposed defects also explain the streaking effects observed by single crystal X-ray diffraction and by electron diffraction. One of the proposed defects can explain the presence of some V^{5+} in this phase. The amount of V^{5+} found both by titration and by ^{31}P NMR spin echo mapping correlates well with defect concentration. The NMR studies also confirm that the V^{5+} present is associated with $(VO)_2P_2O_7$ rather than a second phase. The defects are most prominent in samples prepared to be optimum catalysts for the oxidation of *n*-butane to maleic anhydride. Our work suggests a new explanation for the fact that good VPO catalysts must be prepared by dehydration of a $V_2P_2O_9 \cdot xH_2O$ precursor.

INTRODUCTION

The catalyst used for the commercial production of maleic anhydride by oxidation *n*-butane is a vanadium phosphate (VPO) (1–3). In a laboratory reactor, this catalyst can give maleic anhydride with a selectivity exceeding 80% (4). No other catalyst is known which can give a selectivity approaching 80% for this reaction. This unique catalyst is basically $(VO)_2P_2O_7$, but it must be prepared in a particular way if it is to be an optimum catalyst. It is prepared from a $V_2P_2O_9 \cdot xH_2O$ precursor which has a layer structure (5) (Fig. 1) and a resultant platy morphology. A topotactic dehydration gives $(VO)_2P_2O_7$ which retains the morphology of the precursor. It has been suggested (6–8) that this synthesis procedure enhances the presence of the crystal faces responsible for the highly selective oxidation of *n*-butane. However, this remains an unproved hypothesis.

The stoichiometry of an optimum VPO catalyst deviates by small, but detectable amounts, from $(VO)_2P_2O_7$. There is a slight excess of P (e.g., P/V = 1.05), and the vanadium oxidation state is slightly greater than 4 (e.g., 4.01). This nonstoichiometry had led some to propose (9, 10) that the VPO catalyst is not single phase. Many optimum selective oxidation catalysts are, in fact, composed of more than one phase. For example, the best catalyst for the oxidation of methanol to formaldehyde is a mixture of $Fe_2(MoO_4)_3$ and MoO_3. The reasons for the mixture in this case are understood (11). For the VPO catalyst however, careful diffraction and electron microscopy studies indicate the presence of a single phase if the catalyst has been allowed to achieve steady state in a catalytic reactor (4). Consequently we have sought defects which might explain the nonstoichiometry of the VPO catalyst.

EXPERIMENTAL

The catalyst precursor, $V_2P_2O_9 \cdot xH_2O$, was synthesized by refluxing V_2O_5 with H_3PO_4 (85%) in a mixture of isobutanol and benzyl alcohol using a P–to–V ratio of 1.2. A typical reaction used 24.7 g of H_3PO_4, 15.6 g of V_2O_5, 250 ml of isobutanol, and 18 ml of benzyl alcohol. After refluxing for 24 h, the solid $V_2P_2O_9 \cdot xH_2O$ was separated by vacuum filtration. This product was washed thoroughly with acetone to remove organic residue from the solid. Before this wash, the organic content was about 5 wt%; after washing, it was less than 0.1 wt%. X-ray diffraction showed single phase $V_2P_2O_9 \cdot xH_2O$.

Conversion of $V_2P_2O_9 \cdot xH_2O$ to $(VO)_2P_2O_7$ was carried out under a variety of conditions (Table 1). The oxygen

[1] To whom correspondence should be addressed.

0022-4596/96 $18.00

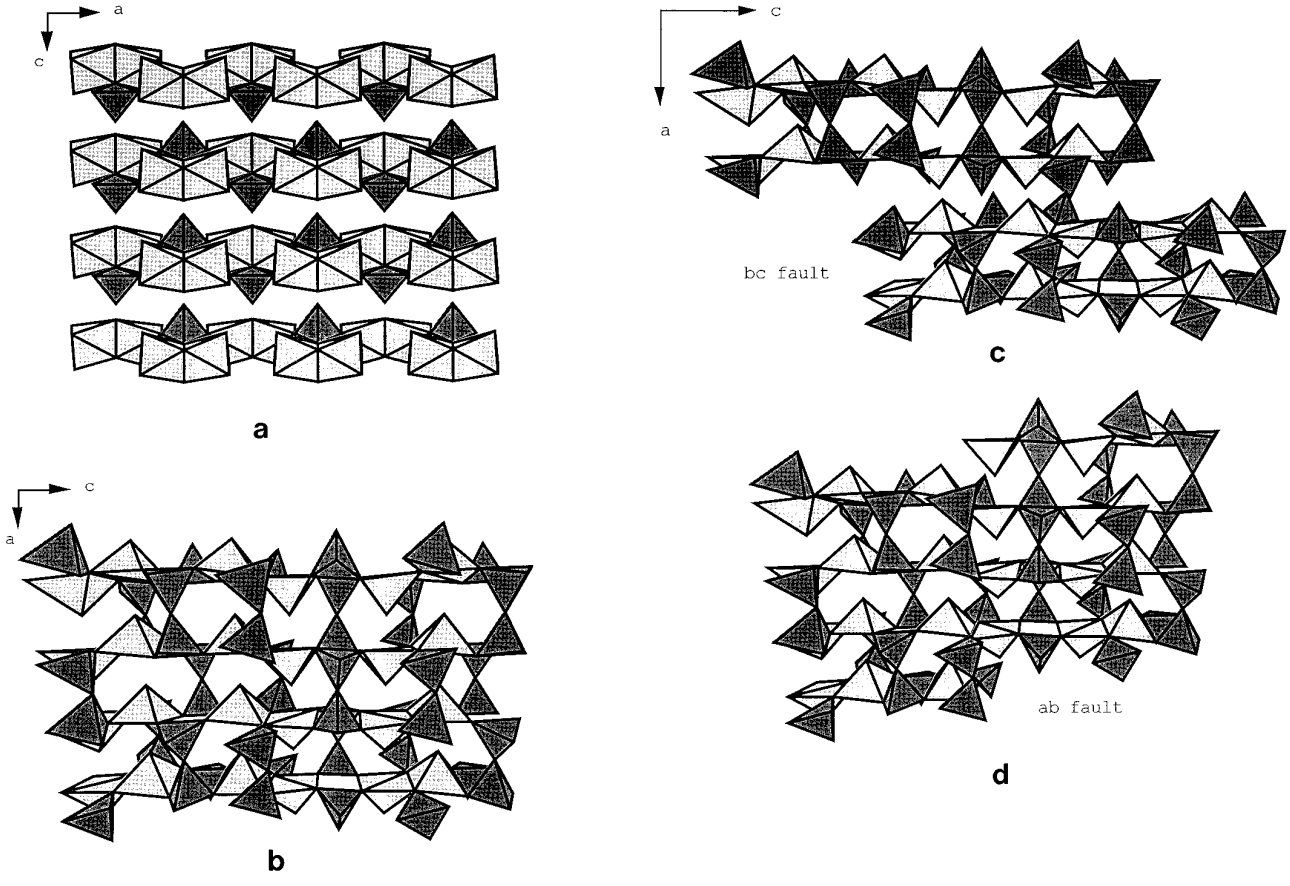

FIG. 1. Dark polyhedra are PO_4 or P_2O_7 groups. Lighter polyhedra are VO_6 or VO_5 groups. (a) Layered precursor structure. (b) Ideal $(VO)_2P_2O_7$ structure. (c) $(VO)_2P_2O_7$ structure with **bc** fault. (d) $(VO)_2P_2O_7$ structure with **ab** fault.

fugacity, $f(O_2)$, during calcination was fixed so that the only product obtained regardless of heating time was $(VO)_2P_2O_7$. The total pressure during this dehydration was about 1 atm; $f(O_2)$ was controlled using either Ar/O_2 or Ar/H_2O mixtures. The gas exiting the furnace was continuously monitored for $f(O_2)$ using a zirconia sensor. The vanadium oxidation state in the products was determined using the method of Nakamura *et al.* (12). The X-ray powder diffraction data were obtained at room temperature with a Siemens D-5000 diffractometer using Cu$K\alpha$ radiation. Strain and crystallite size data given in Table 1 are based on both the Williamson–Hall (13) and Warren–Averback (14) approaches.

The ^{31}P transient NMR experiments were carried out at room temperature on a Chemagnetics/Otsuka CMX-360 spectrometer operating with magnetic field of 8.0 T. Be-

TABLE 1
DIFFaX Simulation Data

Calcination conditions		% **bc**	Fault	Number of	Oxidation	Size	Size	Strain	Strain
Temp.	Time	fault	probability	layers	state	$\|\|$**a**	$\perp$**a**	$\|\|$**a**	$\perp$**a**
400°C	7 days	90	9.5%	7	4.10	197 Å	495 Å	3.3	1.8
645°C	3 days	80	7%	65	4.06	409 Å	1181 Å	2.3	1.5
705°C	24 h	75	3%	500	4.03	928 Å	1020 Å	0.9	0.5
790°C	12 h	70	1%	500	4.01	1367 Å	1394 Å	0.9	0.5
Xtal	12 h	no faults	0%	600	4.00	>1500 Å	>1500 Å	<0.1	<0.1

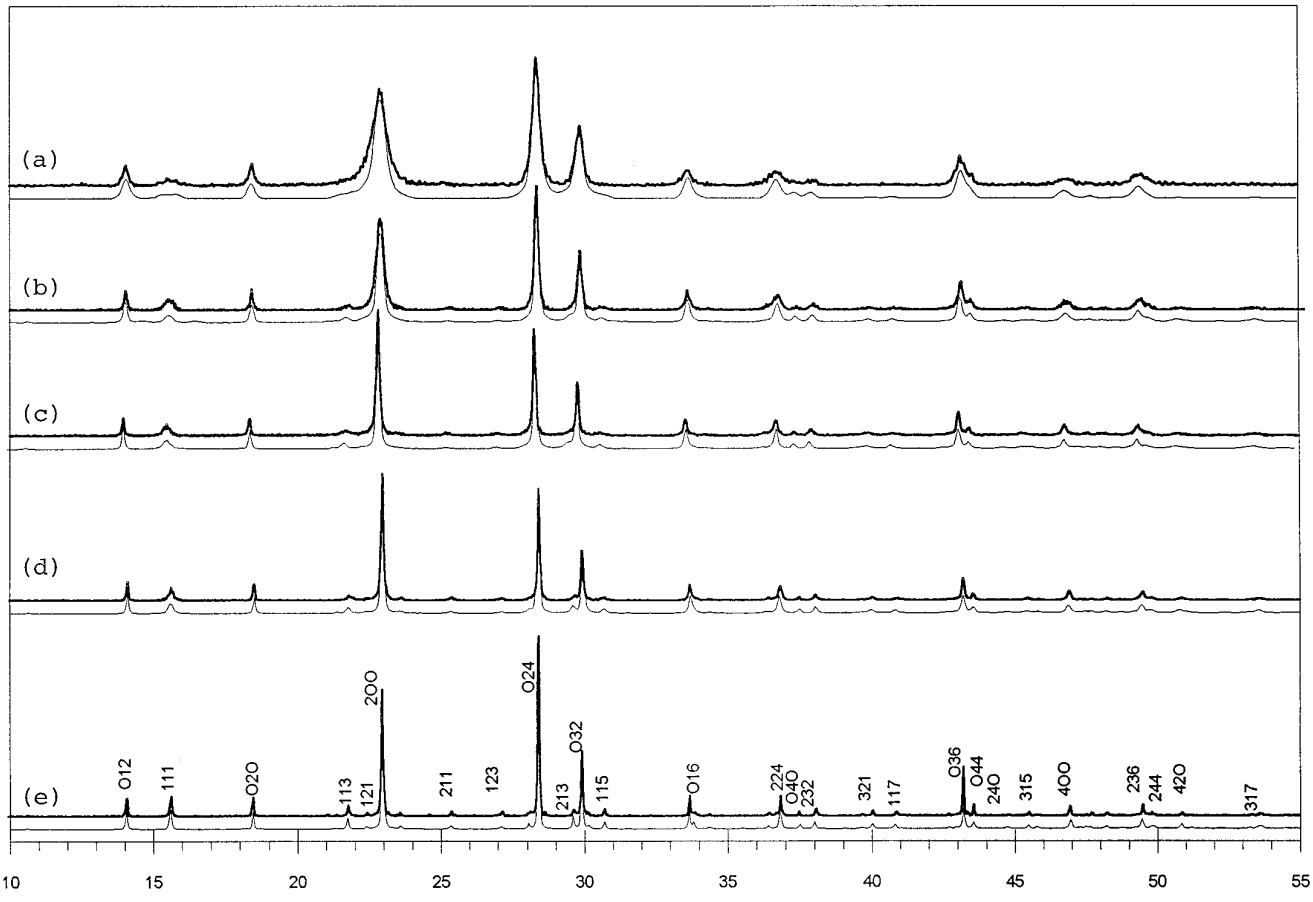

FIG. 2. Observed (dark) and calculated (light) diffraction patterns for $(VO)_2P_2O_7$ prepared under different conditions and described in Table 1. Highest calcination temperature is 400°C for (a), 645°C for (b), 705°C for (c), 790°C for (d), and 900°C for (e).

cause the linewidths generally exceeded the frequency spectrum of the radio-frequency pulses, the method of "spin mapping" (18) was used to obtain spectra. The spin-mapping frequency interval was 50 kHz. Spin-echoes were obtained with a phase-cycled $\pi/2 - \tau - \pi$ pulse sequence where $\tau = 20$ μs. To allow for spin-lattice relaxation, the recycle delay was 40 ms.

RESULTS

Depending on the synthesis conditions used for $(VO)_2P_2O_7$, very different X-ray diffraction patterns can be obtained (Fig. 2). Peak positions, relative to one another, shift by small amounts from sample to sample, but this is a small effect not readily observable in Fig. 2. There are, however, major differences in both peak shapes and the integrated relative intensities of some peaks. Much of the variation in peak shape can be accounted for based on strain and crystallite size effects, after due consideration for the very anisotropic nature of these crystallites (Table 1). In fact, we assume that the broadening of peaks where h and l are both even is due entirely to these strain and size effects. These effects can be estimated along the **a** and **b** axes by using the 200, 400, 020, and 040 reflections. Reflections of the type 00l are too weak to conduct a similar analysis along the **c** axis. However, reflections of the type 0kl where l is even fall into the same pattern as 0k0 reflections, indicating similar parameters along **b** and **c**. Thus, these 0kl reflections are used to estimate strain and crystallite size perpendicular to **a**. The sharper peaks in the upper pattern of Fig. 2 are all 0kl reflections. This should be taken as an indication that the crystallites are considerably larger perpendicular to the **a** direction (Table 1), consistent with their known platy character. The pronounced broadening of the 200 and 400 is an indication of very small crystallite dimensions along the **a** direction.

The extreme broadening of reflections with h or l odd cannot be related to strain or crystallite size effects. The broadening of these reflection can, however, be explained by assuming particular stacking faults perpendicular to the **a** axis (**bc** faults) or perpendicular to the **c** axis (**ab** faults) as shown in Figs. 1a and 1b. The software DIFFaX[15] was

used to calculate the effect of these stacking faults on the X-ray diffraction patterns. Fault **ab** causes broadening of reflections where *l* is odd, whereas fault **bc** causes broadening of peaks where *h* is odd. It was found that a good fit to the observed peak broadening required both **ab** and **bc** faults, although the **bc** fault dominates. The calculated patterns are compared to observed patterns in Fig. 2. The fitting parameters used to calculate these patterns are given in Table 1. The number of layers is defined as the number of unit cells along the **a** or **c** axes. All layers are identical, but the layers are shifted with respect to each other. For a given sample, both faults are calculated with the same stacking fault probability. The broadening and the disappearance of the *hkl* reflections with *h* or *l* odd relates primarily to an increase in the stacking fault density. For the sample prepared at 400°C, an expansion factor of 1.02 was used at the stacking fault. This is necessary to account for the small but significant shifts of peak positions relative to each other. This effect is only noticeable when the stacking fault density is very high. As might be expected, strain parallel and perpendicular to the **a** axis increases (Table 1) as the stacking fault density increases.

Ebner and Thompson (16) reported streaking involving *hkl* reflections where the indices are even–even–odd or even–odd–odd. We find that DIFFaX calculations can simulate these streaks based on our conclusion of a dominant **bc** fault. Bordes and Courtine (8), on the other hand, report in electron diffraction studies streaking along both 100 and 001 directions. We have used DIFFaX to simulate the streaking along 100 with **bc** faults and to simulate the streaking along 001 with **ab** faults. We can, therefore, conclude that a combination of **ab** and **bc** faults explains all the experimental results from electron diffraction and X-ray diffraction and that no simpler defect could explain the observations.

Recently, another type of extended defect was reported (17) to form in VPO catalysts as they age. We have simulated the effect that this 012 fault would have on an X-ray diffraction pattern. We find that this defect cannot produce the observed line broadening and that the line broadening produced by this type of defect is not observed in actual VPO catalysts. This does not indicate the absence of such a defect, but it does show that such defects are present in concentrations much lower than the **ab** and **bc** faults.

Previous studies of VPO catalysts by ^{31}P NMR spin echo mapping have concluded that peaks at ~4650, ~2600, and ~0 ppm are related to V^{3+}, V^{4+} , and V^{5+}, respectively (18–20). However, in no previous study were the spectra correlated with the average state oxidation of vanadium. Our results on some of our samples are shown in Fig. 3. None of these samples shows any evidence of the presence of V^{3+}. The sample which has a very low concentration of defects and no detectable concentration of V^{5+} shows only the one peak related to V^{4+}. None of the previous studies have presented a VPO spectrum without peaks due to V^{3+} or V^{5+}. As the average oxidation state of vanadium increases from 4.00 to 4.01, a peak appears at about 0 ppm. This peak continues to grow as the average vanadium oxidation increases to 4.05 in a sample that appears to be single phase by X-ray diffraction. The sample with an average oxidation state of 4.18 showed $VOPO_4$ as a second phase. The peak near 0 ppm is distinctly different for $VOPO_4$ (Fig. 3e) and VPO samples which do not show a $VOPO_4$ second phase by X-ray diffraction. The non-magnetic character of the P environment of the 0 ppm site in $VOPO_4$ is emphasized by its long spin-lattice relaxation time ($T_1 \sim 20$ s) compared with ^{31}P associated with V^{4+} ($T_1 \sim 20$ ms). The peaks observed near 0 ppm in the two samples shown in Fig. 3b and 3c also exhibit rapid spin-lattice relaxation showing that they are influenced by V^{4+} even though their shifts show that they are most closely associated with V^{5+}. This confirms that the peak near 0 ppm in Figs. 3b and 3c is associated with a V^{5+} defect in $(VO)_2P_2O_7$.

We have explored the nature of line broadening and spectral structure in the V^{4+} line using magic angle spinning NMR (MAS-NMR) at spinning frequencies up to 5500 Hz. These studies revealed a complex structure consisting of a small number of discrete isotropic shifts (sites) whose lines are broadened by the anisotropic shift produced by the paramagnetic V^{4+}. In contrast, we were unable to resolve distinct shifts within the V^{5+} lines near 0 ppm.

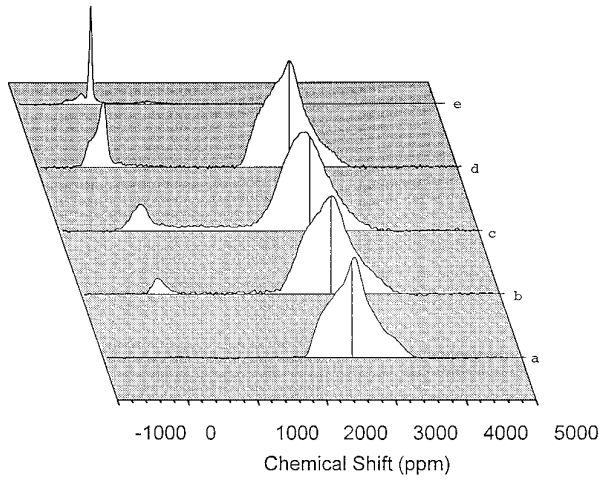

FIG. 3. Spin-mapped ^{31}P NMR spin echo spectra. Chemical shifts were measured relative to a phosphoric acid (85%) reference solution. From bottom to top, the titrations gave vanadium oxidation states of (a) 4.00, (b) 4.01, (c) 4.05, (d) 4.18, and (e) 4.96. X-ray diffraction shows only a $(VO)_2P_2O_7$-type pattern for the samples shown in a–c. Only a $VOPO_4$ pattern was found for the sample shown in e. Both the $(VO)_2P_2O_7$ and $VOPO_4$ phases were evident in the X-ray pattern of the sample shown in d.

DISCUSSION

We have taken special care to produce homogeneous VPO catalysts. Typical VPO catalysts which have been studied are clearly inhomogenous. This inhomogeneity could cause peak broadening features which we wished to avoid because this would complicate our already complex analysis. Inhomogeneities of a VPO catalyst could result either from the way it is used in a reactor or from the way the precursor is transformed to catalyst. A VPO catalyst from a plug-flow, fixed-bed reactor will be exposed to a different temperature and a different gas phase mixture at different regions in the bed. This then could lead to, for example, a different average vanadium oxidation state for catalyst taken from different regions of the reactor. This in turn might have some small, but significant, impact on X-ray peak shapes.

Freshly prepared VPO catalysts are also inhomogeneous when prepared by standard methods. This is caused primarily by the fact that the vanadium oxidation state is not well controlled during a typical conversion of the precursor to the catalyst. Literature reports (1–8, 20, 21, 22) nearly always describe this conversion being carried out under air. At this condition, $(VO)_2P_2O_7$ will eventually be converted completely to VPO_5. Limiting the calcination time can lead to a product where the oxidation state of vanadium is close to 4, but the average oxidation state of vanadium is very likely to be significantly different from particle to particle, with some variation within a particle as well. The most common method of preparing VPO catalysts involves the use of organic chemicals. Normally, these chemicals are not completely removed before calcination. During calcination there are then competing redox processes. Reduction of the vanadium oxidation state to values below 4 may occur by reaction with the organic residue. On the other hand, the vanadium in VPO may be oxidized to values greater than 4 by oxidation with air. Thus, it is likely that during normal precursor conversion, the center of a sample may be initially reduced at the same time that the exterior regions are being oxidized. Recent NMR studies (20) have, in fact, confirmed that different regions of a converted precursor have different oxidation states for vanadium. Dehydration of the precusor under inert gas or vacuum is equally unsatisfactory for producing homogeneous materials because such conditions are actually reducing and tend to produce some V^{3+}.

The usual uncontrolled conversion of precursor $V_2P_2O_9 \cdot xH_2O$ to $(VO)_2P_2O_7$ can apparently diminish the crystallinity of the intermediates in this conversion. Several groups (22) have reported an amorphous intermediate when the crystalline precursor is transformed to crystalline catalyst. We find that this generally occurs if the organic residue is not washed from the catalyst. In our procedure, the organic residue is removed before dehydration of the precursor, and the oxygen partial pressure is controlled throughout the dehydration process. Thus, at no time during the precursor to catalyst conversion is there significant reduction or oxidation of vanadium. X-ray diffraction of our partially converted VPO suggests that there is no intermediate amorphous phase. Partially converted materials instead always show a mixture of crystalline $V_2P_2O_9 \cdot xH_2O$ and $(VO)_2P_2O_7$. Thus, we believe that the transformation is truly topotactic and that our samples are highly homogeneous. It should be emphasized that some line broadening during a topotactic reaction is expected. As a particular crystallite transforms, it will contain domains of both precursor and product. These domains will necessarily be smaller than the original crystallite. Thus, line broadening will result from both the smaller domains and the strain produced in such mixed particle. In the extreme, such effects will cause a disappearance of the Bragg peaks in an X-ray diffraction pattern during the intermediate stages of a topotactic reaction, but such a disappearance is not evidence that the reaction is not topotactic in nature. In the topotactic dehydration, a single crystal of $V_2P_2O_9 \cdot xH_2O$ is converted to a single crystal of $(VO)_2P_2O_7$ without change in morphology.

Despite the uniqueness and importance of the vanadium phosphate catalyst for butane oxidation, this catalyst remains poorly understood. Part of the problem is due to the nature of any alkane oxidation reaction. The first step of activating butane is the step that is rate limiting in the overall oxidation reaction. This then precludes studying butane chemisorption or examining reaction intermediates on the surface of the catalyst. However, aside from the difficulty of understanding the mechanism of butane oxidation, there has been a problem of defining the bulk and surface structures and compositions of the catalyst. This catalyst is routinely prepared with a considerable excess of phosphorus, yet there is only a slight excess of phosphorus in the final catalyst. This excess phosphorus is likely at the surface (9). The vanadium oxidation state in a catalyst that has come to steady state in a catalytic reactor is always slightly greater than 4 (3). Furthermore, if a VPO catalyst is used to oxidize *n*-butane in the absence of oxygen, the oxidation state of vanadium is not noticeably lowered by the time at which selective oxidation ceases (6, 23). This suggests that most of the V^{5+} is associated with defects within the bulk of $(VO)_2P_2O_7$.

A discussion of the defects in $(VO)_2P_2O_7$ must first start with a description of the ideal, defect-free structure. Two independent reports of this structure were given in 1979 (24, 25). The basic structural features (Fig. 1) are double V–O chains along the **a** axis with P_2O_7 groups linking the chains together. Vanadium may be described as octahedrally coordinated to oxygen, but with a strong vanadyl-type distortion. Thus, V–O distances along the **a** axis alternate long (~2.36 Å) or short (~1.60 Å) with four intermediate equatorial V–O distances (~1.95 Å). The long V–O

bond is not shown in Fig. 1. Thus, in Fig. 1, square pyramidal polyhedra are used to describe the environment around vanadium. These pyramids point either up or down along the **a** axis. These units share edges in pairs; the apexes of these two pyramids of this pair point in opposite directions. The original refinements of the $(VO)_2P_2O_7$ structure did not give completely satisfactory agreement between observed and calculated structure factors ($R \sim 18$ to 9%). Thompson and Ebner (16) have achieved better agreement between observed and calculated structure factors ($R \approx 0.035$) by distributing each vanadium atom over two different crystallographic sites only 0.2 Å apart. Problems with typical $(VO)_2P_2O_7$ crystals have been attributed to defects or disorder. Diffuse spots and streaks have been reported in both electron diffraction and single crystal X-ray diffraction patterns (8, 16). We have obtained $(VO)_2P_2O_7$ crystals which give diffraction patterns devoid of streaking effects. This has allowed us to refine the structure to a low R value (3.1%) without introducing any disorder or defects (26). We find that the actual space group is monoclinic rather than one of the orthorhombic space groups (*Pcam*, *Pcaa*, or $Pca2_1$) that had been considered previously. Our more precise definition of the ideal structure does not, however, alter the basic structural features of $(VO)_2P_2O_7$ as shown in Fig. 1.

During the topotactic transformation of $V_2P_2O_9 \cdot xH_2O$ to $(VO)_2P_2O_7$, there is ample opportunity for stacking faults to occur. The precursor crystal structure is a layered structure with no V–O or P–O bonds bridging the layers. These layers (Fig. 1a) are held together only by van der Waals and hydrogen bonding. As the water is removed during the topotactic reaction, both V–O and P–O bonds form across the layers where there were previously no such bonds. Mistakes can be made as these layers become strongly bound to each other. The lower the temperature of calcination, the more likely it is that stacking faults occur. This is demonstrated by our DIFFaX calculations (Table 1 and Fig. 2). The **bc** stacking fault can be described as a change in orientation of the vanadyl distortion resulting in a switch from –V=O–V=O–V= chains to =V–O=V–O=V– chains at the stacking fault boundary. At the **ab** fault boundary, there is no alteration of the double vanadyl chains; however, there is a change in the pattern of the pyrophosphate groups (Fig. 1).

The observed vanadium oxidation state increases with decreasing calcination temperature (Table 1). This might be attributed either to a higher surface area or to a higher defect concentration. However, the vanadium oxidation state in a VPO catalyst is always higher than 4.00 even after precautions have been taken to avoid an oxidized surface. For example, a VPO catalyst which has been reacted with pure butane until selective oxidation ceases still shows a vanadium oxidation state higher than 4.00 (6, 23). In fact, the oxidation state of vanadium has not changed within the accuracy of the titrations. Furthermore, we find that the vanadium oxidation state of a given VPO catalyst does not change significantly after equilibration at oxygen fugacities differing by several orders of magnitude. Thus, it seems likely that the amount of V^{5+} in a VPO catalyst is primarily associated with some defect in the bulk, rather than being mainly associated with the surface. Analysis of $(VO)_2P_2O_7$ magnetic susceptibility data also leads to the conclusion that the V^{5+} in VPO is associated with a defect in the bulk of $(VO)_2P_2O_7$ rather than a second V^{5+} containing phase (27). This conclusion is further confirmed by the NMR results presented in this paper.

A possible explanation for the presence of some V^{5+} in $(VO)_2P_2O_7$ is that not all $(PO_4)^{4-}$ groups dimerize during the topotatic transformation. In fact, the **bc** stacking fault (Fig. 1) apparently prevents the formation of some pyrophosphate groups across the fault. This could lead then to a formula of the type $(V^{4+}_{1-2x}V^{5+}_{2x}O)_2(P_2O_7)_{1-x}(PO_4)_{2x}$ at the **bc** stacking fault. If the apical oxygens of the VO_5 square pyramids are not shared between two such units, there is even more excess oxygen and thus more V^{5+}. This stacking fault therefore can readily rationalize all or a substantial fraction of the V^{5+} found in VPO catalysts. No change in composition or oxidation state is expected due to **ab** faults.

The extended defects found in VPO catalysts may be directly related to its catalytic properties. The best catalysts are those where these defects are very prominent. This suggests the possibility that the active sites for selective *n*-butane oxidation are associated with regions where the extended defects meet the surface. Since there is currently no accurate way to determine the number of active sites at the surface, this hypothesis cannot be checked at this time.

ACKNOWLEDGMENTS

This work was supported by E. I. du Pont de Nemours, Inc. and by NSF DMR-9305780.

REFERENCES

1. P. N. Rylander and W. J. Zimmerscheid, U.S. Patent 2,773,921 (1956).
2. A. W. Sleight, *Catal. Today* **1,** 347 (1987).
3. G. Centi, F. Trifiro, J. R. Ebner, and V. M. Franchetti, *Chem. Rev.* **88,** 55 (1988).
4. R. M. Contractor, H. E. Bergna, H. S. Horowitz, C. M. Blackstone, U. Chowdhry, and A. W. Sleight, *in* "Catalysis 1987" p. 645. Elsevier, Amsterdam, 1988.
5. C. C. Torardi and J. C. Calabrese, *Inorg. Chem.* **23,** 1308 (1984).
6. R. M. Contractor, H. E. Bergna, H. S. Horowitz, C. M. Blackstone, B. Malone, C. C. Torardi, B. Griffiths, U. Chowdhry, and A. W. Sleight, *Catal. Today* **1,** 49 (1987).
7. H. S. Horowitz, C. M. Blackstone, A. W. Sleight, and G. Teufer, *Appl. Catal.* **38,** 193 (1988).
8. E. Bordes and P. Courtine, *J. Catal.* **57,** 236 (1979).
9. G. Bergeret, J. P. Broyer, M. David, P. Gallezot, J. C. Volta, and G. J. Hecquet, *Chem. Soc. Chem. Commun.* 825 (1986).

10. B. K. Hodnett, *Catal. Rev. Sci. Eng.* **27,** 373 (1985).
11. C. J. Machiels and A. W. Sleight, *in* ''Proceedings of the Fourth International Conference on the Chemistry and Uses of Molybdenum'' (H. F. Barry and P. C. H. Mitchell, Eds.), p. 411. Climax Molybdenum Co., Ann Arbor, MI, 1982; C. J. Machiels, U. Chowdhry, R. H. Staley, F. Ohuchi, and A. W. Sleight, *in* ''Catalytic Conversions of Synthesis Gas and Alcohols to Chemicals'' (R. G. Herman, Ed.), p. 413. Plenum, 1984; A. W. Sleight, *in* ''Solid State Chemistry Compounds'' (A. K. Cheetham and P. Day, Eds.), p. 166. Oxford Univ. Press, London, 1992.
12. N. Nakamura, K. Kawai, and Y. Fujiwara, *J. Catal.* **34,** 345 (1974).
13. G. Williamson and W. H. Hall, *Acta Metall.* **1,** 22 (1953).
14. B. E. Warren and B. L. Averbach, *J. Appl. Phys.* **21,** 595 (1950).
15. J. M. M. Treacy, J. M. Newsam, and M. W. Deem, *Proc. R. Soc. London A* **433,** 499 (1991).
16. J. R. Ebner and M. R. Thompson, ''Studies in Surface Science and Catalysis'' (R. K. Grasselli and A. W. Sleight, Eds.), p. 31. Elsevier, Amsterdam, 1992.
17. P. L. Gai and K. Kourtakis, *Science* **267,** 661 (1995).
18. J. Li, M. E. Lashier, G. L. Schrader, and B. C. Gerstein, *Appl. Catal.* **73,** 83 (1991).
19. M. T. Sananes, A. Tuel, and J. C. Volta, *J. Catal.* **145,** 251 (1994).
20. M. T. Sananes, A. Tuel, G. J. Hutchings, and J. C. Volta, *J. Catal.* **148,** 395 (1994).
21. J. C. Vedrine, J. M. M. Millet, and J. C. Volta, *Faraday Discuss. Chem. Soc.* **87,** 207 (1989).
22. P. Amoros, R. Ibanez, A. Beltran, D. Beltran, A. Fuertes, P. Gomez–Romero, E. Hernandez, and J. Rodriquez–Carvajal, *Chem. Mater.* **3,** 407 (1991); F. Cavani and F. Trifiro, *Chemtech.* April (1994).
23. R. M. Contractor and A. W. Sleight, *Catal. Today* **3,** 175 (1988).
24. Yu. E. Gorbunova and S. A. Linde, *Sov. Phys. Dokl.* **24,** 138 (1979).
25. N. E. Middlemiss, PhD. Thesis, McMaster University, Hamilton, Ontario, Canada, 1978.
26. P. T. Nguyen, R. D. Hoffman, and A. W. Sleight, *Mater. Res. Bull.* **30,** 1055 (1995).
27. J. W. Johnson, D. C. Johnston, A. J. Jacobson, and J. F. Brody, *J. Am. Chem. Soc.* **106,** 8123 (1984).